
Proceedings Paper:
von den Driesch, N, Stange, D, Wirths, S et al. (8 more authors) (2016) Direct bandgap GeSn light emitting diodes for short-wave infrared applications grown on Si. In: Proceedings of SPIE. SPIE Photonics West - OPTO, Silicon Photonics XI (Conference 9752), 15-17 Feb 2016, San Francisco, California, USA. Society of Photo-optical Instrumentation Engineers (SPIE) .

https://doi.org/10.1117/12.2211641

Direct bandgap GeSn light emitting diodes for short-wave infrared applications grown on Si

Nils von den Driesch[a], Daniela Stange[a], Stephan Wirths[a], Denis Rainko[a], Gregor Mussler[a], Toma Stoica[a,b], Zoran Ikonic[c], Jean-Michel Hartmann[d], Detlev Grützmacher[a], Siegfried Mantl[a], and Dan Buca[a]

[a]Peter Grünberg Institute (PGI 9) and JARA-Fundamentals of Future Information Technologies, Forschungszentrum Jülich, Germany
[b]National Institute of Materials Physics, Magurele, Romania
[c]Institute of Microwaves and Photonics, School of Electronic and Electrical Engineering, University of Leeds, United Kingdom
[d]CEA, LETI, MINATEC Campus and Univ. Grenoble Alpes, France

ABSTRACT

The experimental demonstration of fundamental direct bandgap, group IV GeSn alloys has constituted an important step towards realization of the last missing ingredient for electronic-photonic integrated circuits, i.e. the efficient group IV laser source. In this contribution, we present electroluminescence studies of reduced-pressure CVD grown, direct bandgap GeSn light emitting diodes (LEDs) with Sn contents up to 11 at.%. Besides homojunction GeSn LEDs, complex heterojunction structures, such as GeSn/Ge multi quantum wells (MQWs) have been studied. Structural and compositional investigations confirm high crystalline quality, abrupt interfaces and tailored strain of the grown structures. While also being suitable for light absorption applications, all devices show light emission in a narrow short-wave infrared (SWIR) range. Temperature dependent electroluminescence (EL) clearly indicates a fundamentally direct bandgap in the 11 at.% Sn sample, with room temperature emission at around 0.55 eV (2.25 μm). We have, however, identified some limitations of the GeSn/Ge MQW approach regarding emission efficiency, which can be overcome by introducing SiGeSn ternary alloys as quantum confinement barriers.

Keywords: GeSn, Direct bandgap, Optoelectronics, Light emitting diodes, Multi quantum wells, Silicon photonics

1. INTRODUCTION

Monolithic integration of photonics with the well-known Si-CMOS technology may be an attractive solution for future energy-efficient computing. Especially silicon or groupIV photonics, the application of silicon and germanium as materials for optical components, is thought to be key technology due to its compatibility with microelectronics fabrication processes.[1]

However, elemental Si and Ge are indirect bandgap semiconductors and therefore poor choices for light-emitting devices. Recently, cubic GeSn, an alloy made solely from group IV materials, has been shown to become a fundamentally direct semiconductor for Sn concentrations above approx. 9 at.% Sn.[2] On the other hand, compressive strain in tetragonal GeSn is known to strongly impact this indirect-to-direct transition[3] since it decreases the so-called directness, i.e. the difference between indirect L- and direct Γ-valley. Thus the required Sn concentration for the transition shifts towards higher Sn values, making strain relaxed structures desirable. While this important breakthrough has already led to the demonstration of optically pumped lasing at low temperatures,[2] an electrically driven light source is needed for on-chip applications.

While GeSn LEDs already showed advantages compared to elemental Ge LEDs,[4] different schemes have been

Further author information:
N.v.d.D.: E-mail: n.von.den.driesch@fz-juelich.de
D.B.: E-mail: d.m.buca@fz-juelich.de

explored to increase their efficiency. GeSn homojunction LEDs were fabricated, with a beneficial lack of defective interfaces in the active region.[5] Ge/GeSn/Ge double heterostructures (DHS) were also demonstrated, offering a higher carrier confinement.[6,7]
From the successful history of III-V light emitters,[8] the future path towards more efficient group IV light emitting devices can be envisaged. To begin with, heterostructures spatially confine carriers more efficiently in the optically active region. Furthermore, the reduced density of states in lower dimensional structures, such as quantum wells or quantum dots, may lead to a remarkable decrease of the required lasing threshold current densities.[8] First results on electroluminescence (EL) from GeSn/Ge multi quantum wells (MQWs) have been published.[9,10]
In our contribution, we report on the electrical characterization and on EL measurements of GeSn LEDs with several designs using low current densities, i.e. ¡ 100 A/cm2. Homojunction LEDs with 8 at.% and 11 at.% Sn are compared and investigated by means of temperature dependent EL. Performance of a seven well GeSn/Ge MQW LED with 8 at.% Sn is studied and the limits of this heterostructure approach explored. Finally, beneficial impacts stemming from the introduction of ternary SiGeSn alloys are theoretically investigated, while the epitaxial feasibility of this strategy is demonstrated.

2. METHODS

2.1 Epitaxy

Epitaxy of different light emitting device stacks was performed in a 200 mm reduced-pressure chemical vapor deposition (CVD) reactor (AIXTRON), with a showerhead design for homogeneous gas distribution above the whole wafer. In order to minimize lattice mismatch between Si(001) substrate and GeSn epilayers, growth is performed on top of 2.5μm thick Ge virtual substrates (Ge-VS), grown previously in a different reactor.[11] Commercially available precursor gases such as digermane (Ge_2H_6) and tintetrachloride ($SnCl_4$) were employed for growth of the GeSn-based heterostructures. The use of higher order hydrides as well as chlorine-containing gases enables growth at temperatures well below 400°C, which represents a crucial requirement for incorporation of large amounts of substitutional Sn atoms into the crystal.[12,13] To allow the formation of electron and hole injection layers into the active device region, in-situ doping by phosphine (PH_3) and diborane (B_2H_6) gases was performed during epitaxy of the device layers. Compared to ion implantation, this approach yields a large density of activated dopants, while avoiding implantation-induced damages and the necessity of thermal annealing steps. The LED structures were grown using two different schemes: GeSn homojunctions with Sn concentrations of 8 at.% and 11 at.% Sn, respectively. (b) GeSn quantum wells in the active region. In both designs, the bottom layer consists of a partially strain relaxed, in-situ doped GeSn buffer layer, serving as a carrier injection layer into the active region as well. This buffer helps releasing residual compressive strain (coming naturally from growth on Ge VS) in the device layers above and, thus, increasing their directness. Therefore, a larger number of carriers populate the direct Γ-valley, leading to more efficient light emission. Since the growth of the full p-i-n layer stacks leads to total thicknesses well above the critical thickness for strain relaxation, misfit dislocations will start to appear near the GeSn/Ge interface. The use of a partially relaxed bottom layer ensures the formation of these defects well below the intrinsic region, preventing the occurrence of non-radiative recombination centers directly at the interface with the active GeSn region.
The active device region is on top of that bottom in-situ doped GeSn layer. In case of the homojunction structures, it simply consists of an undoped GeSn layer exhibiting the same Sn concentration as the injection layer below. In case of the multi quantum well device, the active region consists of seven GeSn quantum wells with Sn concentrations of about 8 at.% and thicknesses of about 20 nm. The barrier layers in-between consist of elemental Ge, with thicknesses around 14 nm. Since elemental Ge and GeSn noticeably differ in terms of lattice constants, the GeSn wells are still compressively strained (by about -0.71%), while the Ge barriers have a tensile strain of about 0.48%. The inhomogeneous strain distribution in the MQW region will have an impact on device performance, as discussed later on.
All device structures end up with an about 60 nm thick in-situ doped GeSn layer, which serves as a carrier injection layer and which is contrarily doped compared to the bottom one.

2.2 Device fabrication

Fabrication of LEDs in various structural designs was performed using only the standard Si CMOS compatible technology. Due to the metastability of the GeSn alloys, emphasis was put on a low thermal budget during all

processing steps. Structuring of the device mesas was performed by Cl_2/Ar based reactive ion etching (RIE). The subsequent mesa passivation was carried out using a two-step approach. A conformal 10 nm thick layer of Al_2O_3 was deposited at 300°C by atomic layer deposition (ALD), followed by 150 nm of SiO_2 obtained from plasma-enhanced chemical vapor deposition (PECVD) at 300°C. Contact opening by optical lithography and RIE enables the formation of low ohmic NiGeSn contacts[14] by sputtering of Ni with subsequent forming gas annealing at 325°C. Finally, for contacting the devices, an additional 200 nm thick Al layer was deposited.

2.3 Electroluminescence Measurements

EL measurements were performed using a Bruker VERTEX 80 V FTIR spectrometer system, employing the system's step scan mode. The samples were mounted in a cryostat, which can be cooled with liquid He to access a temperature range between 4 K and room temperature. Light emission was induced by pulsed voltage excitation at a frequency of around 2 kHz with a 70% duty cycle. The emitted light was collected into a liquid nitrogen cooled InSb detector, while the influence of thermal radiation was further minimized by using a cutoff filter at about 3 μm.

3. RESULTS AND DISCUSSIONS

A cross-sectional transmission electron microscopy (TEM) micrograph, depicted in Figure 1(a), shows the structural quality of a GeSn homojunction structure with 8 at.% Sn, hereafter denoted as sample A (see Table 1). A large number of misfit dislocations can be seen at the interface between the Ge-VS and the bottom GeSn layer, caused by strain relaxation in the about 500 nm thick device structure. However, these defects seem to be confined at the interface, as no threading dislocations can be seen in the TEM micrograph penetrating into the active region. This behavior is very beneficial, since threading dislocations are known to form midgap traps[15] that seriously degrade the device performance. Still, dislocation half loops penetrate into the Ge-VS, which on the other hand does not impact light emission efficiency in the active region.

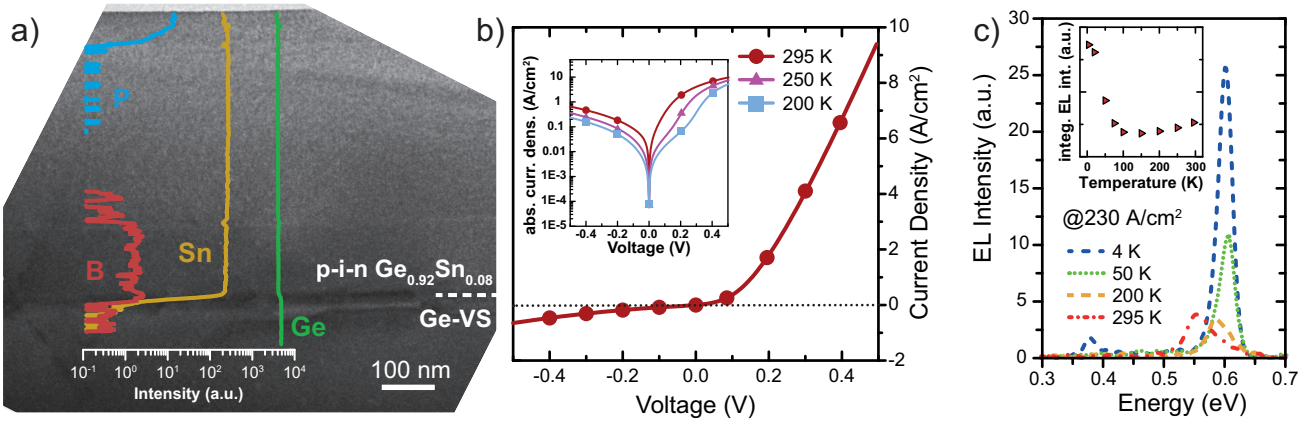

Figure 1. (a): TEM micrograph of sample A, a GeSn homojunction LED, overlaid with SIMS spectra. (b) I-V curves of the same structure. (c) Temperature dependent EL spectra, along with integrated EL intensity vs. temperature (inset).

In contrast to the TEM micrograph, a clear distinction between the differently doped regions can be made in the overlaid secondary ion mass spectrometry (SIMS) profiles. Both phosphorus and boron atoms are found solely in the top and bottom layers, respectively, without diffusion into the active layer. Steep interfaces originate from the low temperature used during epitaxy, well below 400°C. No impact of diborane and phosphine on Sn incorporation during the growth process is observed. This observation is in contrast to the results in,[16] where a strong Sn concentration change was noticed after introduction of boron precursors.

I-V curves have been acquired to identify suitable operation regions of the device. Clear forward and reverse bias regimes can be identified in room temperature measurements, as shown in Fig. 1(b). Therefore the devices, being light emitters in forward regime, are in principle also able to act as light detectors under reversed bias, as shown for GeSn in different detector designs.[17–19] In the inset, the same measurement is shown in log-log

scale also for lower temperatures. A clear curving in the forward regime can be observed when lowering the temperature down to 200 K. This curving is linked to a regime of negative differential resistance, which has already been observed in similar GeSn devices at temperatures below about 140 K.[20]
Temperature dependent EL spectra between 4 K and 295 K are shown in Fig. 1(c), where two trends can be seen. While the 4 K EL peak is located at about 603 meV (2.066 μm), it clearly shifts to smaller energies of around 552 meV (2.246 μm) when heating up to room temperature. This shift of 50 meV is linked to a temperature related bandgap narrowing, well described by a quadratic Varshni-Fit (not shown here). The small feature, occurring slightly below 0.40 eV in the low temperature spectrum, is also observed in low temperature PL spectra[3] and may be related to defects at the GeSn/Ge interface. The second important outcome of the experiment can be seen in the inset of Fig 1(c), where the integrated EL intensity is plotted against temperature. When lowering the temperature, the integrated intensity first of all decreases. Below about 100 K, it starts to strongly increase again. This behavior is caused by a combination of two different effects. The GeSn material used for sample A indeed exhibits an indirect bandgap, with a difference between the indirect L- and the direct Γ-valley of about 10 meV. Therefore, when the measurement temperature is lowered, excited electrons condense into the minimum L valley, decreasing radiative recombination efficiency. On the other hand, modelling results (Supplementary Information of Ref.[2]) indicate that the non-radiative carrier lifetime in the material sharply increases from several hundred ps (RT) towards the ns regime at temperatures below 100 K. Therefore efficiency degradation due to non-radiative electron-hole recombination is strongly reduced at very low temperatures, leading to a distinct EL emission increase. Still, a true direct bandgap material is required for efficient room temperature light emission. In the following, we present data on sample B, a GeSn LED with a higher incorporated Sn concentration of 11 at.% (Details in Table 1).

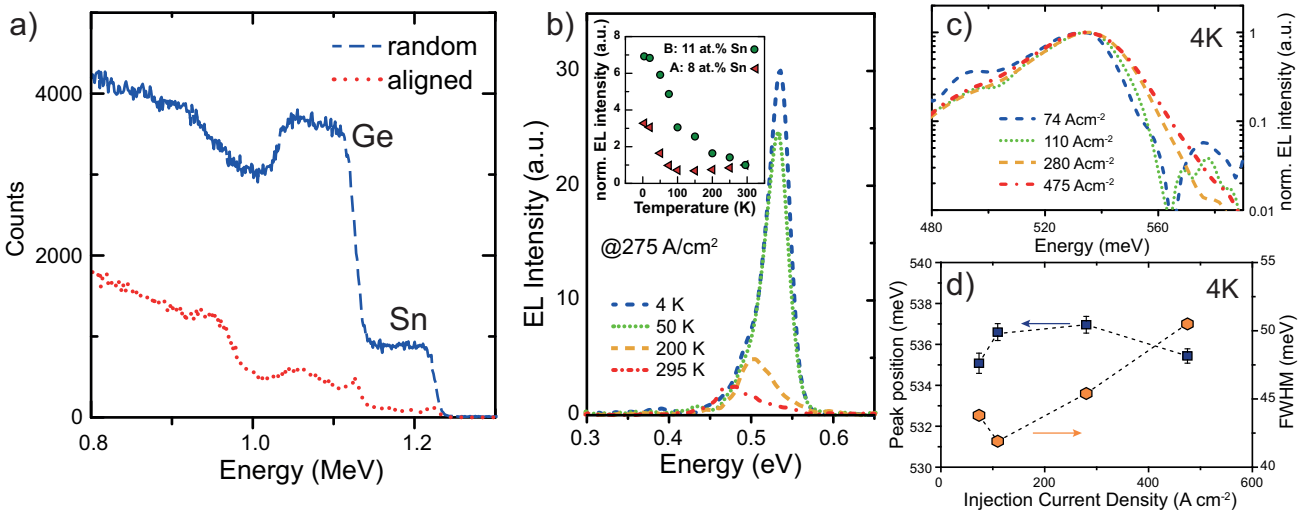

Figure 2. (a): RBS spectrum of sample B. (b): Temperature dependent EL spectra, and integrated EL intensity in comparison with sample A (inset). (c): Normalized current density dependent EL spectra at 4 K for sample B. (d): Injection current density dependent shift in EL peak position and FWHM at 4 K in sample B.

To check the crystalline quality of the about 270 nm thick sample B, Rutherford Backscattering Spectroscopy (RBS) measurements employing 1.4 MeV He^+ ions have been performed in both random and crystal aligned geometry, as shown in Fig. 2(a). The onset of signal below about 1.23 MeV is linked to Sn atoms, while the onset below 1.12 MeV is related to Ge atoms from the GeSn layer. Compared to the random one, the measurement in crystal channeling direction is strongly reduced, indicating a high atom substitutionality for Ge and Sn atoms in the GeSn layer. The appearance of so called surface peaks in the channeling spectrum indicate a smooth surface, e.g. without Sn precipitates. Since RBS spectra indicate a high crystalline layer quality, temperature dependent EL spectra have been acquired and shown in Fig. 2(b). Similarly to sample A, a peak shift from 471 meV (room temperature) up to 536 meV (4K) together with a strong intensity increase can be observed in sample B when reducing measurement temperature. The temperature dependence of normalized EL intensity is shown for samples A and B in the inset of Fig. 2(b). In contrast to sample A, sample B shows a continuous EL

signal increase. This behavior can be explained by the fundamental direct bandgap of the material in sample B. Electrons once again accumulate in the lowest energy valley, which now is the -valley, leading to an EL emission increase. As in sample A, the additional low temperature light emission increase may be explained by the strong increase in non-radiative lifetime that hampers such deleterious recombinations.

To learn more about the required injected current densities as well as associated heating effects, EL measurements were performed at various injection current densities at 4 K. The required current density in order to obtain measurable EL spectra is found to be well below 100 A/cm^2, comparable to reference.[6] Normalized EL measurements for injection current densities between 74 A/cm^2 and 475 A/cm^2 are depicted on a logarithmic scale in Fig. 2(c). While the peak position itself does not seem to be influenced by the current density, the tail towards higher energies increases for higher injected currents. The high energy tail reflects the Boltzmann distribution of carriers. Therefore a wider tail is linked to a higher carrier temperature, induced by the high injected currents, and mirrors itself in an increasing Full Width at Half Maximum (FWHM), as shown in Fig. 2(d). However, no sign of temperature-induced bandgap narrowing is observed, since the EL peak position hardly changes in Fig. 2(d), e.g. compared to reference.[4] Part of this effect may be compensated by an increased band filling from the higher injection currents. Still, we conclude that heating effects coming from the increase of the current densities in our probed range are small indeed.

The very successful history of III-V lasers indicates important guide lines in order to increase the efficiency of these devices.[8] One important step is the reduction of the active region's dimensionality. The decreased density of states in for instance 2D quantum wells, indeed led to a massive reduction of the current density required to achieve the lasing threshold. Therefore, we have also studied EL in a GeSn/Ge multi quantum well device, denoted in the following as sample C, layer properties of which can be found in Table 1.

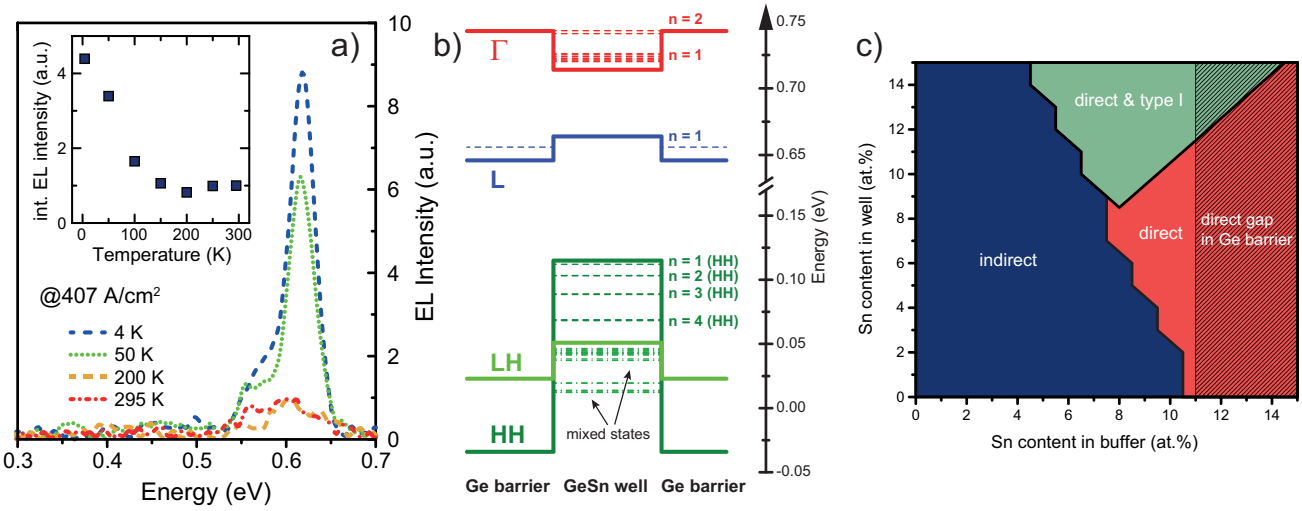

Figure 3. (a): Temperature dependent EL spectra of MQW sample C. (b): Calculated band alignment in sample C. (c): Representation of suitable parameter regions from calculated band alignments.

Temperature dependent EL spectra are shown in Fig. 3(a). Since the active layer's Sn concentration is comparable to sample A, the peak position at room temperature is similar, at around 593 meV (versus 552 meV for sample A), while the energy difference is due to the larger amount of residual compressive strain of -0.71% in this sample (see Table 1). The integrated peak intensity increase as temperature decreases, provided in the inset of Fig. 3(a), again indicates an indirect bandgap in the active layer. This indication is backed up by band structure calculations of the device, using a k·p and deformation potential model to account for strain, as in,[21] applying material parameters from the supporting information of Ref.[2] To check on the device's quantized states, calculations were performed using the effective mass method for the conduction band, while employing a 6-band k·p model for the valence band.[22] The results, shown in Fig 3(b), offer rather surprising electronic band alignments, lacking a type I alignment in conduction band. While Γ electrons are confined with a barrier height of 29 meV, confinement in the L band is inverted. Tensile strain in the Ge interlayers (see Table 1), induced by the partially relaxed GeSn buffer, reduces the L valley to an energy position 18 meV below that in GeSn. Therefore

the majority of electrons is located in the Ge barrier rather than in the GeSn, as intended. However, all holes are confined within the GeSn layers, with barrier heights of 81 meV for heavy holes (HH) states and 28 meV for light holes (LH). Still, most offsets are small compared to thermal energy at room temperature ($k_BT \sim 25$ meV). Those small offsets, along with the ineffective electron confinement, make our GeSn/Ge LED a rather inefficient device. The interplay between residual compressive strain in GeSn wells and tensile strain in Ge barriers not only affects this device, but is relevant for all high Sn content GeSn devices employing with elemental Ge as barrier material. To highlight this, we performed thorough band structure calculations for such heterostructures, the results are provided in Fig. 3(c). For that purpose we assumed a fully strain relaxed GeSn buffer layer with Sn concentration between 0 and 15 at.%, a practically accessible parameter space for CVD growth. On top of that buffer, which dictates the overall strain in the active layers, we modelled a GeSn/Ge quantum well with Sn contents in the well once again between 0 and 15 at.%. Here, we only consider band alignments between the GeSn well and elemental Ge barriers, e.g. we neglected quantization effects. Our calculations result in a variety of alignment behaviors in the active region. The blue part of the representation in Figure 3(c) is associated with an indirect bandgap behavior in the GeSn well and can thus be considered ineffective for LEDs. In the red part of Fig. 3(c), GeSn wells become fundamentally direct, however, no type I band alignment is reached, as in sample C. Additionally, for Sn concentrations in the buffer above 11 at.%, the induced tensile strain in the elemental Ge barriers leads to a direct bandgap transition in those as well (black shaded region). Although band engineering of Ge also is a well-known alternative for group IV optoelectronics,[23,24] its small bandgap interferes with our integration scheme; the black shaded part can thus be ruled out, as well. Only the orange area of the representation features both a direct GeSn alloy, as well as a suitable type I band alignment. However, in this parameter space, a maximum electron confinement of 40 meV (Γ-valley) and 41.4 meV (L-valley) at room temperature can be reached. Hence our integration scheme, using elemental Ge barriers, will not confine electrons effectively. When going towards quantum well structures, quantization effects are expected to reduce carrier confinement even further.

An already investigated[25,26] alternative is the introduction of ternary alloys as barriers. We performed theoretical calculations to prove its suitability in the limited accessible parameter space. For that purpose bandgaps, deformation potentials and effective masses were taken from,[26] with average valence band offsets of constituents again from.[27] Bandgap bowing for GeSn is taken from[28] and for SiSn and SiGe from.[29] The required Luttinger parameters were calculated in two steps. First, the ones for the GeSn binaries are calculated, as described in the SI of,[2] and then linear interpolation is used for Si(GeSn).

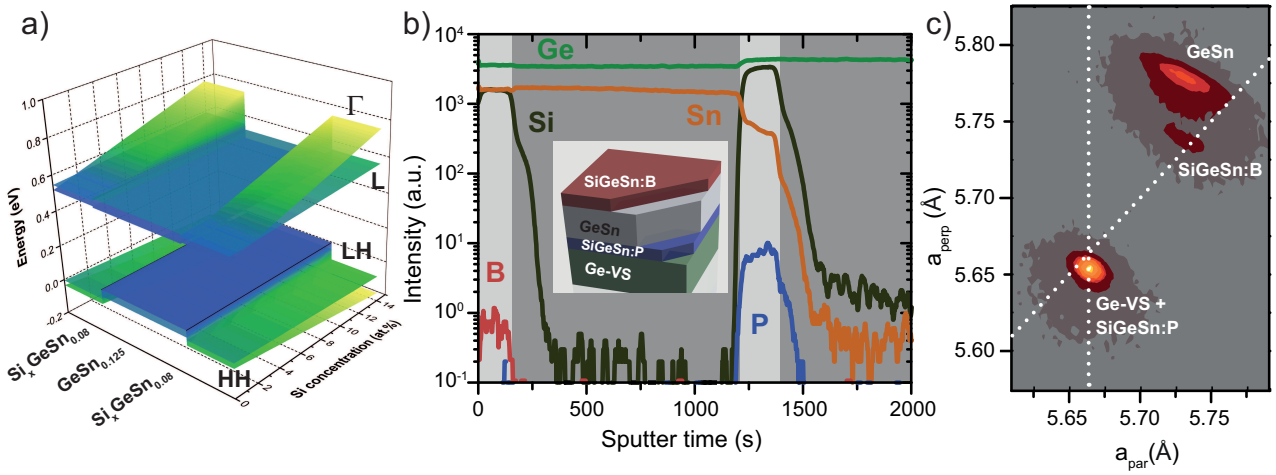

Figure 4. (a): Band alignment for SiGeSn/GeSn heterostructures for varying Si contents. SIMS data (b) and XRD (c) measurements on a SiGeSn/GeSn/SiGeSn DHS.

Practically reachable band alignments are shown for SiGeSn/GeSn Double Heterostructures (DHS) in Fig. 4(a). We assume an active GeSn layer with 12.5 at.% Sn and a residual compressive strain of -0.40% and SiGeSn claddings coherently grown to it. SiGeSn claddings have a fixed Sn concentration of 8 at.%, a realistic value related to the necessary low temperature growth, and varying Si concentration between 0 and 14 at.%. Our

calculations show, for 14 at.% Si in the ternary alloy barriers, a confinement of 388 meV for Γ- and 67 meV for L-electrons, much stronger than in the elemental Ge case.
To show the feasibility of our approach we have grown a SiGeSn/GeSn/SiGeSn double heterostructure, sample D, as schematically depicted in the inset of Fig. 4(b). From a growth point of view, the main difficulties are the low temperature growth of the top SiGeSn cladding layer, due to the limited thermal budget of the layer stack. A second important issue is the in-situ doping of both cladding layers. SIMS analysis of sample D, shown in Fig. 4(b), substantiate the possibility of such growth scheme. The boron doped SiGeSn layer with 11 at.% Sn and 8 at.% Si on top, as well as the phosphorus doped SiGeSn layer with 4 at.% Sn and 15 at.% Si at the bottom are clearly distinguishable regions in the device.
XRD analysis of sample D in Fig. 4(c) provide information on strain distribution inside the device. The signal of the bottom ternary cladding layer overlays the one from the Ge-VS, since it was grown lattice matched. The active GeSn region with 12.3 at.% is partially relaxed, with a residual compressive strain of -0.47 %. The boron doped cladding on top is grown coherently onto the GeSn layer, since their in-plane lattice constant exactly match. Therefore no additional defects at the upper interface of the active region are introduced, which is beneficial for efficient light emission.

Table 1. Overview on investigated samples

Sample	Structure	Active region: Sn content (at.%)	Active region: Strain (%)	Active region: Thickness (nm)	Total stack thickness (nm)
A	GeSn homojunction	8	-0.18	345	504
B	GeSn homojunction	11	-0.8	102	272
C	7x GeSn/Ge MQW	7.8/-	-0.71/0.48	7x 21/14	450
D	SiGeSn/GeSn DHS	12.3	-0.47	423	543

4. SUMMARY AND OUTLOOK

In conclusion, we have performed growth and electro-optical characterization of several GeSn homojunction and Ge/GeSn multi quantum well LEDs. Strong light emission at low injection current densities was observed for samples with 8 at.% and 11 at.% Sn at 0.60 eV (2.07μm) and 0.55 eV (2.55μm), respectively. Furthermore a clear indication of a fundamentally direct bandgap in the latter case was observed by temperature dependent EL measurements.
Narrow light emission from a GeSn/Ge MQW heterostructure LED indicates the suitability of more complex designs for future energy-efficient Si photonics light emitters. However, as shown by band structure calculations, the current GeSn/Ge approach is limited by the inefficient electron confinement in the active region (approx. 40 meV, at most). Introduction of ternary SiGeSn alloys as confinement barriers, in the experimentally accessible parameter space as theoretically and practically demonstrated, may be a solution due to much higher carrier confinements.

ACKNOWLEDGMENTS

This research received funding for CVD growth investigations from Federal Ministry of Education and Research (BMBF) under project UltraLowPow (16ES0060 K). The authors also acknowledge funding from The Royal Society International Exchanges grant IE131593. We furthermore thank Steffi Lenk for her assistance with TEM measurements.

REFERENCES

[1] Soref, R., "Mid-infrared photonics in silicon and germanium," *Nature Photonics* **4**(8), 495–497 (2010).
[2] Wirths, S., Geiger, R., von den Driesch, N., Mussler, G., Stoica, T., Mantl, S., Ikonic, Z., Luysberg, M., Chiussi, S., Hartmann, J. M., Sigg, H., Faist, J., Buca, D., and Grützmacher, D., "Lasing in direct-bandgap GeSn alloy grown on Si," *Nature Photonics* **9**, 88–92 (2015).

[3] Stange, D., Wirths, S., von den Driesch, N., Mussler, G., Stoica, T., Ikonic, Z., Hartmann, J. M., Mantl, S., Grützmacher, D., and Buca, D., "Optical transitions in direct-bandgap Ge1 x Snx alloys," *ACS Photonics* **2**(11), 1539–1545 (2015).

[4] Oehme, M., Kostecki, K., Arguirov, T., Mussler, G., Ye, K., Gollhofer, M., Schmid, M., Kaschel, M., Korner, R. A., Kittler, M., Buca, D., Kasper, E., and Schulze, J., "GeSn heterojunction LEDs on Si substrates," *IEEE Photonics Technology Letters* **26**(2), 187–189 (2014).

[5] Gallagher, J. D., Senaratne, C. L., Xu, C., Sims, P., Aoki, T., Smith, D. J., Menéndez, J., and Kouvetakis, J., "Non-radiative recombination in Ge1ySny light emitting diodes: The role of strain relaxation in tuned heterostructure designs," *Journal of Applied Physics* **117**(24), 245704 (2015).

[6] Du, W., Zhou, Y., Ghetmiri, S. A., Mosleh, A., Conley, B. R., Nazzal, A., Soref, R. A., Sun, G., Tolle, J., Margetis, J., Naseem, H. A., and Yu, S.-Q., "Room-temperature electroluminescence from Ge/Ge1-xSnx/Ge diodes on Si substrates," *Applied Physics Letters* **104**(24), 241110 (2014).

[7] Tseng, H. H., Wu, K. Y., Li, H., Mashanov, V., Cheng, H. H., Sun, G., and Soref, R. a., "Mid-infrared electroluminescence from a Ge/Ge0.922Sn0.078/Ge double heterostructure p-i-n diode on a Si substrate," *Applied Physics Letters* **102**(18), 182106 (2013).

[8] Alferov, Z., "Double heterostructure lasers: Early days and future perspectives," *IEEE Journal on Selected Topics in Quantum Electronics* **6**(6), 832–840 (2000).

[9] Stange, D., von den Driesch, N., Rainko, D., Schulte-Braucks, C., Wirths, S., Mussler, G., Tiedemann, A. T., Stoica, T., Hartmann, J. M., Ikonic, Z., Mantl, S., Grützmacher, D., and Buca, D., "Study of GeSn based heterostructures: towards optimized group IV MQW LEDs," *Optics Express* **24**(2), 1358 (2016).

[10] Schwartz, B., Oehme, M., Kostecki, K., Widmann, D., Gollhofer, M., Koerner, R., Bechler, S., Fischer, I. A., Wendav, T., Kasper, E., Schulze, J., and Kittler, M., "Electroluminescence of GeSn/Ge MQW LEDs on Si substrate," *Optics Letters* **40**(13), 3209 (2015).

[11] Hartmann, J., Abbadie, A., Cherkashin, N., Grampeix, H., and Clavelier, L., "Epitaxial growth of Ge thick layers on nominal and 6 off Si(001); Ge surface passivation by Si," *Semiconductor Science and Technology* **24**(5), 055002 (2009).

[12] von den Driesch, N., Stange, D., Wirths, S., Mussler, G., Holländer, B., Ikonic, Z., Hartmann, J. M., Stoica, T., Mantl, S., Grützmacher, D., and Buca, D., "Direct bandgap group IV epitaxy on Si for laser applications," *Chemistry of Materials* **27**(13), 4693–4702 (2015).

[13] Wirths, S., Buca, D., Mussler, G., Tiedemann, A. T., Holländer, B., Bernardy, P., Stoica, T., Grützmacher, D., and Mantl, S., "Reduced pressure CVD growth of Ge and Ge1-xSnx alloys," *ECS Journal of Solid State Science and Technology* **2**(5), N99–N102 (2013).

[14] Wirths, S., Troitsch, R., Mussler, G., Hartmann, J.-M., Zaumseil, P., Schroeder, T., Mantl, S., and Buca, D., "Ternary and quaternary Ni(Si)Ge(Sn) contact formation for highly strained Ge p- and n-MOSFETs," *Semiconductor Science and Technology* **30**(5), 055003 (2015).

[15] Gupta, S., Simoen, E., Vrielinck, H., Merckling, C., Vincent, B., Gencarelli, F., Loo, R., and Heyns, M., "Identification of Deep Levels Associated with Extended and Point Defects in GeSn Epitaxial Layers Using DLTS," *ECS Transactions* **53**(1), 251–258 (2013).

[16] Vincent, B., Gencarelli, F., Bender, H., Merckling, C., Douhard, B., Petersen, D. H., Hansen, O., Henrichsen, H. H., Meersschaut, J., Vandervorst, W., Heyns, M., Loo, R., and Caymax, M., "Undoped and in-situ B doped GeSn epitaxial growth on Ge by atmospheric pressure-chemical vapor deposition," *Applied Physics Letters* **99**(15), 152103 (2011).

[17] Oehme, M., Widmann, D., Kostecki, K., Zaumseil, P., Schwartz, B., Gollhofer, M., Koerner, R., Bechler, S., Kittler, M., Kasper, E., and Schulze, J., "GeSn/Ge multiquantum well photodetectors on Si substrates.," *Optics Letters* **39**(16), 4711–4714 (2014).

[18] Oehme, M., Kostecki, K., Schmid, M., Kaschel, M., Gollhofer, M., Ye, K., Widmann, D., Koerner, R., Bechler, S., Kasper, E., and Schulze, J., "Franz-Keldysh effect in GeSn pin photodetectors," *Applied Physics Letters* **104**(16), 161115 (2014).

[19] Gassenq, A., Gencarelli, F., Van Campenhout, J., Shimura, Y., Loo, R., Narcy, G., Vincent, B., and Roelkens, G., "GeSn/Ge heterostructure short-wave infrared photodetectors on silicon," *Optics express* **20**(25), 27297 (2012).

[20] Schulte-Braucks, C., Stange, D., von den Driesch, N., Blaeser, S., Ikonic, Z., Hartmann, J. M., Mantl, S., and Buca, D., "Negative differential resistance in direct bandgap GeSn p-i-n structures," *Applied Physics Letters* **107**(4), 042101 (2015).

[21] Menendez, J. and Kouvetakis, J., "Type-I GeGe1xySixSny strained-layer heterostructures with a direct Ge bandgap," *Applied Physics Letters* **85**(7), 1175 (2004).

[22] Shun Lien Chuang, "Physics of optoelectronic devices," Wiley-Interscience (1995).

[23] Süess, M. J., Geiger, R., Minamisawa, R. A., Schieer, G., Frigerio, J., Chrastina, D., Isella, G., Spolenak, R., Faist, J., and Sigg, H., "Analysis of enhanced light emission from highly strained germanium microbridges," *Nature Photonics* **7**, 466–472 (2013).

[24] Sukhdeo, D. S., Nam, D., Kang, J.-H., Brongersma, M. L., and Saraswat, K. C., "Direct bandgap germanium-on-silicon inferred from 5.7% 100 uniaxial tensile strain [Invited]," *Photonics Research* **2**(3), A8–A13 (2014).

[25] Sun, G., Soref, R. A., and Cheng, H. H., "Design of a Si-based lattice-matched room-temperature GeSn/GeSiSn multi-quantum-well mid-infrared laser diode.," *Optics express* **18**(19), 19957–19965 (2010).

[26] Chang, G.-E., Chang, S.-W., and Chuang, S. L., "Strain-Balanced GezSn1-z/SixGeySn1-x-y Multiple-Quantum-Well Lasers," *IEEE Journal of Quantum Electronics* **46**, 1813–1820 (dec 2010).

[27] Jaros, M., "Simple analytic model for heterojunction band offsets," *Physical Review B* **37**(12), 7112–7114 (1988).

[28] Ryu, M. Y., Harris, T. R., Yeo, Y. K., Beeler, R. T., and Kouvetakis, J., "Temperature-dependent photoluminescence of Ge/Si and Ge1-ySny/Si, indicating possible indirect-to-direct bandgap transition at lower Sn content," *Applied Physics Letters* **102**, 171908 (2013).

[29] Moontragoon, P., Soref, R. A., and Ikonic, Z., "The direct and indirect bandgaps of unstrained SixGe1xySny and their photonic device applications," *Journal of Applied Physics* **112**(7), 073106 (2012).